

# **Elementary Decomposition Mechanisms of Lithium Hexafluorophosphate in Battery Electrolytes and Interphases**

Evan Walter Clark Spotte-Smith,<sup>†,‡,⊥</sup> Thea Bee Petrocelli,<sup>†,‡,¶,⊥</sup> Hetal D. Patel,<sup>†,‡</sup> Samuel M. Blau,<sup>§</sup> and Kristin A. Persson<sup>\*,‡,||</sup>

*†Materials Science Division, Lawrence Berkeley National Laboratory, 1 Cyclotron Road, Berkeley, CA, 94720 USA*

*‡Department of Materials Science and Engineering, University of California, Berkeley, 210 Hearst Memorial Mining Building, Berkeley, CA, 94720 USA*

*¶Cabrillo College, 6500 Soquel Drive, Aptos, CA, 95003 USA*

*§Energy Storage and Distributed Resources, Lawrence Berkeley National Laboratory, 1 Cyclotron Road, Berkeley, CA, 94720 USA*

*||Molecular Foundry, Lawrence Berkeley National Laboratory, 1 Cyclotron Road, Berkeley, CA, 94720 USA*

*⊥These authors contributed equally to this work*

E-mail: kapersson@lbl.gov

## **Abstract**

Electrolyte decomposition constitutes an outstanding challenge to long-life Li-ion batteries (LIBs) as well as emergent energy storage technologies, contributing to protection via solid electrolyte interphase (SEI) formation and irreversible capacity loss over a battery's life. Major strides have been made to understand the breakdown of

common LIB solvents; however, salt decomposition mechanisms remain elusive. In this work, we use density functional theory to identify the decomposition of lithium hexafluorophosphate ( $\text{LiPF}_6$ ) salt under SEI formation conditions. Our results suggest that  $\text{LiPF}_6$  forms  $\text{POF}_3$  primarily through rapid chemical reactions with  $\text{Li}_2\text{CO}_3$ , while hydrolysis should be kinetically limited at moderate temperatures. We further find that the proposed autocatalysis of  $\text{POF}_3$  is selective and that  $\text{POF}_3$  preferentially reacts with highly charged oxyanions. These results indicate a means of interphase design in LIBs, suggesting that  $\text{LiPF}_6$  reactivity may be controlled by varying the abundance or distribution of inorganic carbonate species or by limiting the transport of  $\text{PF}_6^-$  through the SEI.

Lithium-ion batteries (LIBs) have in recent years become a cornerstone energy storage technology,<sup>1</sup> powering not just personal electronics but also a growing number of electric vehicles. To continue this trend of electrification in transportation and other sectors, LIBs with higher energy density<sup>2–5</sup> and longer cycle and calendar life<sup>6</sup> are needed, motivating research into novel battery materials. Battery electrolytes, which are typically the limiting factor in terms of LIB potential window and irreversible capacity loss,<sup>7–9</sup> are an especially attractive target for research and development to expand the utility of LIBs. In today's commercial LIBs, the most common electrolytes are comprised of lithium hexafluorophosphate ( $\text{LiPF}_6$ ) dissolved in blends of cyclic carbonates, especially ethylene carbonate (EC), and linear carbonates such as ethyl methyl carbonate.<sup>10–14</sup> Carbonate/ $\text{LiPF}_6$  electrolytes have many desirable properties, including weak ion association and high  $\text{Li}^+$  conductivity,<sup>15–17</sup> but they are reactive at low potentials. When paired with graphite negative electrodes, carbonate/ $\text{LiPF}_6$  electrolytes decompose to form a relatively stable passivation film known as the solid electrolyte interphase (SEI),<sup>18–23</sup> which prevents continual electrolyte degradation while allowing reversible charging and discharging. On the other hand, conventional electrolytes based on EC and  $\text{LiPF}_6$  are essentially incompatible with high-energy density negative electrodes (e.g. Li metal,<sup>24,25</sup> Si<sup>26,27</sup>) and form unstable SEIs, resulting in compar-

atively poor cycle and calendar life.<sup>28,29</sup>

Due to the significance of the SEI in preserving battery capacity, SEI formation from carbonate/LiPF<sub>6</sub> electrolytes has been extensively studied for decades.<sup>30–32</sup> Such studies have sought to reveal the fundamental processes involved in the exemplar carbonate/LiPF<sub>6</sub> system and to identify opportunities for improvement through electrolyte engineering. An understanding of the decomposition of carbonate solvents, particularly EC, has been developed through both experiment and theory. In addition to characterizing a wide range of decomposition products - including gases,<sup>33,34</sup> short-chain organic molecules, oligomers/polymers, and inorganic carbonates (e.g. Li<sub>2</sub>CO<sub>3</sub>) and oxides (e.g. Li<sub>2</sub>O)<sup>19</sup> - plausible elementary mechanisms for EC decomposition have been identified using density functional theory (DFT),<sup>35–37</sup> *ab initio* molecular dynamics (AIMD),<sup>38–40</sup> and chemical reaction network analysis.<sup>41–44</sup>



In comparison, there are many open questions concerning the decomposition of LiPF<sub>6</sub>. It is widely accepted that LiPF<sub>6</sub> decomposes to form LiF, which precipitates and contributes to the SEI.<sup>30,31,45,46</sup> A range of other products, including POF<sub>3</sub>,<sup>47</sup> difluorophosphoric acid (PF<sub>2</sub>OOH),<sup>48</sup> and some organophosphorus compounds<sup>49</sup> have been identified by experimental spectroscopy. Moreover, LiPF<sub>6</sub> demonstrates thermal instability,<sup>50,51</sup> and it has long been suggested that an autocatalytic decomposition mechanism involving POF<sub>3</sub> (Equations 1-2) is responsible.<sup>52</sup> However, mechanistic explanations for LiPF<sub>6</sub> decomposition remain lacking. Most commonly, hydrolysis<sup>7,45,46,51,53</sup> is invoked to explain observed PF<sub>6</sub><sup>-</sup> decomposition (Equations 3-4 show an example mechanism). LiPF<sub>6</sub> has been shown to be unstable in the presence of water,<sup>14</sup> yet hydrolysis alone is insufficient to explain the significant role of LiPF<sub>6</sub> in SEI formation. The DFT study of Okamoto<sup>54</sup> suggests that PF<sub>6</sub><sup>-</sup> hydrolysis should

be extremely slow, in agreement with longstanding experimental evidence.<sup>55</sup> Moreover, LIB electrolytes used in laboratory studies are often rigorously dried, allowing  $\sim$ 10 ppm H<sub>2</sub>O. Though exposure to high potentials on the positive electrode can both enable the formation of H<sub>2</sub>O by reactions with EC<sup>56</sup> and accelerate PF<sub>6</sub><sup>-</sup> hydrolysis,<sup>57</sup> this cannot explain LiF formation or further LiPF<sub>6</sub> decomposition during early SEI formation before high potentials have been reached or in batteries without high-voltage positive electrodes.



In this work, we explore the decomposition mechanisms of LiPF<sub>6</sub> using DFT at a high level of theory (see Supporting Information for details). We find that water is not necessary to explain the formation of LiF or POF<sub>3</sub>, but rather that PF<sub>5</sub> can react rapidly with readily available Li<sub>2</sub>CO<sub>3</sub> during early SEI formation. This mechanism is entirely chemical in nature; it does not depend on electrochemical reduction or oxidation of LiPF<sub>6</sub> and can occur at any depth of the SEI as long as the transport of PF<sub>6</sub><sup>-</sup> to inorganic carbonate domains is feasible. Hence, porosity, morphology and transport properties of the SEI also becomes a relevant factor. We then study POF<sub>3</sub> autocatalysis, using PF<sub>2</sub>OOH and LiPF<sub>2</sub>O<sub>2</sub> as model intermediates. Due to selective reactivity between POF<sub>3</sub> and highly charged oxyanions, LiPF<sub>2</sub>O<sub>2</sub> is preferred over PF<sub>2</sub>OOH in the absence of an oxidizing potential. Our calculations additionally indicate that overall, the POF<sub>3</sub> autocatalytic cycle is limited by a slow intramolecular fluorine transfer step. These findings answer longstanding questions regarding the reactivity of LiPF<sub>6</sub> and suggest new routes for controlling salt reactivity during SEI formation.

**Decomposition of LiPF<sub>6</sub> to POF<sub>3</sub>:** We begin by considering the formation of PF<sub>5</sub>, which is a key intermediate in essentially all LiPF<sub>6</sub> reaction routes considered in the literature and in this work. We find that the elimination of LiF from LiPF<sub>6</sub> to form PF<sub>5</sub> (Equation

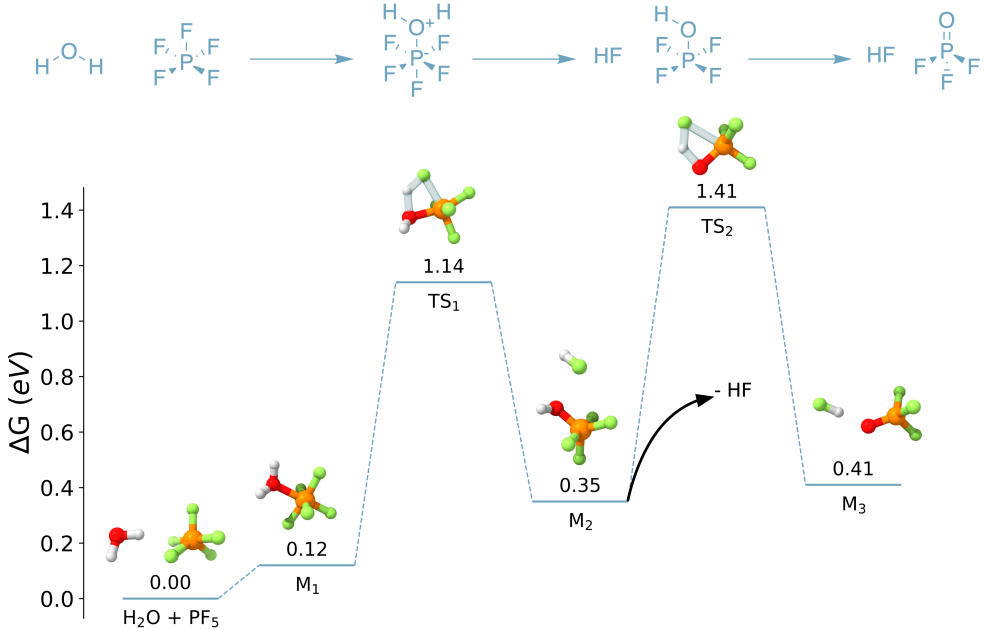


Figure 1: Hydrolysis of  $\text{PF}_5$  to form  $\text{POF}_3$  and 2 HF. This mechanism is overall thermodynamically unfavorable and involves two reactions with high barriers ( $\Delta G^\ddagger > 1.00 \text{ eV}$ ).

3) has no transition-state but is endergonic, with  $\Delta G = 1.04 \text{ eV}$ . However, we note that the product in this reaction is a solution-phase molecule of LiF, whereas we expect that LiF will precipitate, forming solid deposits within the SEI. This reaction is more likely to occur when considering the possibility that LiF could be stabilized by precipitation. Okamoto<sup>54</sup> previously found that the deposition of solid LiF ( $\text{LiF}(\text{solv}) \longrightarrow \text{LiF}(\text{solid})$ ) has  $\Delta G = -1.17 \text{ eV}$ , which would make Equation 3 overall exergonic. More recently, Cao et al.<sup>58</sup> used DFT and AIMD to show that  $\text{LiPF}_6$  decomposition by either chemical or electrochemical means is greatly accelerated in the presence of existing LiF. Here, we report the reaction energies and energy barriers of LiF elimination reactions like Equation 3 without including the effect of a surface or LiF precipitation. However, we emphasize that we expect these reactions, in general, to be more favorable than what is predicted based on calculations with molecular LiF in solution.

Even once  $\text{PF}_5$  is formed, Figure 1 confirms that, at our chosen level of theory, the direct hydrolysis of  $\text{PF}_5$  by  $\text{H}_2\text{O}$  is unfavorable. Each of the three hydrolysis steps - the addition

of  $\text{H}_2\text{O}$  to  $\text{PF}_5$  ( $\text{H}_2\text{O} + \text{PF}_5 \longrightarrow \text{M}_1$ ), the elimination of HF to form  $\text{PF}_4\text{OH}$  ( $\text{M}_1 \longrightarrow \text{M}_2$ ), and the elimination of HF from  $\text{PF}_4\text{OH}$  ( $\text{M}_2 \longrightarrow \text{M}_3$ ) - is predicted to be endergonic. Further, the latter two steps both have energy barriers  $\Delta G^\ddagger > 1.00$  eV, agreeing with the experimental observation that hydrolysis is slow at room temperature. Significant thermal activation beyond temperatures reached in normal LIB cycling conditions would be required to enable  $\text{LiPF}_6$  hydrolysis.

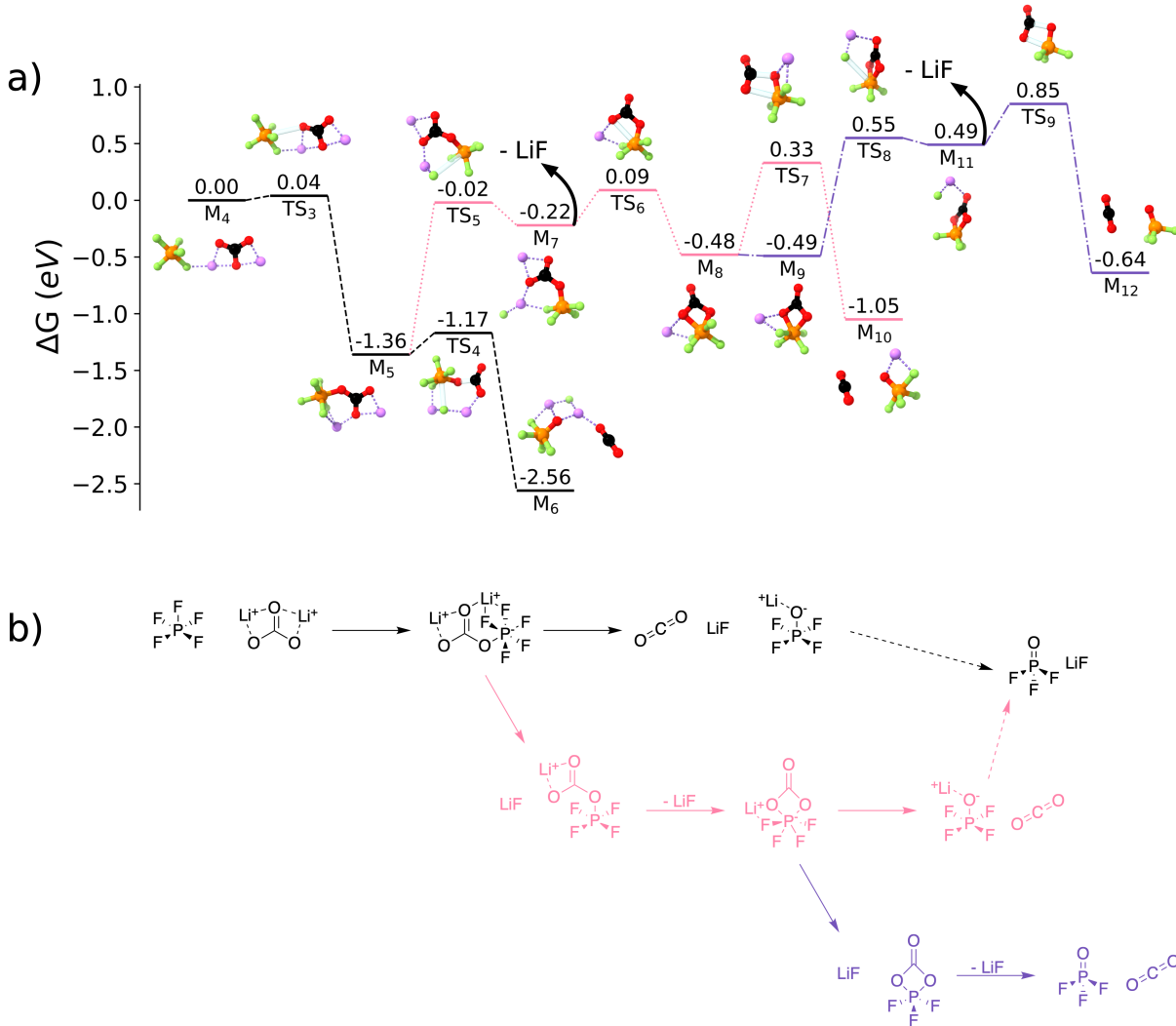


Figure 2: Energy diagram (a) and scheme (b) for the reaction between  $\text{PF}_5$  and  $\text{Li}_2\text{CO}_3$  to form  $2\text{LiF}$ ,  $\text{CO}_2$ , and  $\text{POF}_3$ . In the black and pink paths,  $\text{LiPOF}_4$  is formed (M<sub>6</sub>, M<sub>10</sub>).  $\text{LiPOF}_4$  can decompose to form  $\text{LiF}$  and  $\text{POF}_3$  with  $\Delta G^\ddagger = 0.63$  eV,  $\Delta G = 0.28$  eV, but this is not shown in (a) (see Supporting Information).

An alternate mechanism involves the reaction of  $\text{PF}_5$  with  $\text{Li}_2\text{CO}_3$  (Figure 2). Reactions

between  $\text{PF}_5$  and inorganic carbonates have been proposed in the past<sup>59,60</sup> on the basis of the observed evolution of  $\text{CO}_2$  and  $\text{POF}_3$  upon mixing of  $\text{LiPF}_6$  and  $\text{Li}_2\text{CO}_3$ , but this route has largely been neglected in favor of hydrolytic mechanisms. Moreover, to the best of our knowledge, this mechanism has never been studied by first-principles calculations.

We find that  $\text{PF}_5$  reacts vigorously with  $\text{Li}_2\text{CO}_3$ . An initial addition step between the two reactants ( $M_4 \longrightarrow M_5$ ) has a low barrier of  $\Delta G^\ddagger = 0.04$  eV. The adduct ( $M_5$ ) then dissociates in a single concerted reaction, yielding  $\text{LiF}$ ,  $\text{CO}_2$ , and  $\text{LiPOF}_4$  with  $\Delta G^\ddagger = 0.20$  eV. Finally, to form  $\text{POF}_3$ ,  $\text{LiPOF}_4$  eliminates an additional molecule of  $\text{LiF}$ , with  $\Delta G^\ddagger = 0.63$  eV,  $\Delta G = 0.28$  eV (not shown in Figure 2; see Supporting Information). We again note that we expect both  $\Delta G$  and  $\Delta G^\ddagger$  for  $\text{LiF}$  elimination reactions to be lowered if precipitation of  $\text{LiF}$  on a surface is allowed. Even without any corrections for the instability of molecular  $\text{LiF}$  produced in  $M_5 \longrightarrow M_6$  and  $\text{LiPOF}_4 \longrightarrow \text{LiF} + \text{POF}_3$ , this mechanism represents one of the most thermodynamically and kinetically favorable elementary mechanism for  $\text{PF}_5$  decomposition yet reported.

If it does not dissociate completely, the adduct  $M_5$  may instead eliminate  $\text{LiF}$  ( $M_5 \longrightarrow M_7$ ), though this reaction suffers from a high predicted barrier of  $\Delta G^\ddagger = 1.34$  eV. After  $\text{LiF}$  elimination, an additional oxygen from the carbonate group binds to phosphorus to form a ring complex  $M_8$ . By eliminating  $\text{CO}_2$ , either immediately ( $M_8 \longrightarrow M_{10}$ ,  $\Delta G^\ddagger = 0.81$  eV) or following the elimination of another  $\text{LiF}$  ( $M_{11} \longrightarrow M_{12}$ ,  $\Delta G^\ddagger = 0.36$  eV), this ring complex also forms  $\text{LiPOF}_4$  ( $M_{10}$ ) or  $\text{POF}_3$  ( $M_{12}$ ).

The proposed mechanisms shown in Figure 2 rely only on  $\text{Li}_2\text{CO}_3$ , which should be abundant at the negative electrode, especially during early SEI formation.<sup>21,31,38,60–62</sup> The reaction of  $\text{PF}_5$  and  $\text{Li}_2\text{CO}_3$  is also entirely chemical in nature; none of the reactions in Figure 2 depend on electrochemical oxidation or reduction. As a result, the decomposition should not depend explicitly on applied potential, the proximity to the anode surface, or the availability of electrons. Therefore, we predict that the decomposition of  $\text{PF}_5$  can occur anywhere in the SEI, so long as inorganic carbonates like  $\text{Li}_2\text{CO}_3$  are present. This being

said, because  $\text{Li}_2\text{CO}_3$  is formed in the SEI as a result of electrochemical reduction of EC,<sup>38,44</sup> the overall rate of  $\text{POF}_3$  formation via the reaction of  $\text{PF}_5$  with  $\text{Li}_2\text{CO}_3$  will implicitly have a potential dependence.

While our focus in this work is on  $\text{LiPF}_6$  decomposition during SEI formation, it is worth noting that  $\text{Li}_2\text{CO}_3$  is an impurity formed during the synthesis of common transition metal oxide positive electrodes.<sup>59</sup> Accordingly, the mechanisms described in Figure 2 could occur at the positive electrode as well as at the negative electrode or the SEI.

**Autocatalytic decomposition of  $\text{PF}_5$ :** Figure 2 indicates that  $\text{POF}_3$  emerges rapidly by reaction with  $\text{Li}_2\text{CO}_3$  during SEI formation. This hints that the proposed autocatalytic mechanisms for  $\text{POF}_3$  (re)formation (Equations 1-2), which rely on  $\text{POF}_3$  and carbonate species, are chemically plausible.

To confirm the mechanism of  $\text{POF}_3$  autocatalysis at elevated temperature, we first consider the formation of  $\text{PF}_2\text{O}_2\text{R}$  species (Figure 3). Specifically, we explore the formation of  $\text{PF}_2\text{OOH}$  from  $\text{H}_2\text{CO}_3$  (Figure 3a) and  $\text{LiHCO}_3$  (Figure 3b) and the formation of  $\text{LiPF}_2\text{O}_2$  by  $\text{Li}_2\text{CO}_3$  (Figure 3c). In addition to their relevance for  $\text{POF}_3$  formation and  $\text{LiPF}_6$  decomposition,  $\text{PF}_2\text{O}_2\text{R}$  species and in particular difluorophosphoric acid ( $\text{PF}_2\text{OOH}$ ) have been blamed as major contributors to the decomposition of SEI species and the loss of battery capacity.<sup>63,64</sup> Jayawardana et al. have argued that  $\text{PF}_2\text{OOH}$  should form at the positive electrode, as a result of  $\text{PF}_6^-$  oxidation.<sup>63</sup> If  $\text{PF}_2\text{OOH}$  and related species could form at the negative electrode without high potentials, it could have significant implications for the stability of the SEI.

Figure 3a shows a mechanism for a chemical reaction between  $\text{H}_2\text{CO}_3$  and  $\text{POF}_3$ . The initial addition reaction between  $\text{POF}_3$  and  $\text{H}_2\text{CO}_3$  ( $\text{H}_2\text{CO}_3 + \text{POF}_3 \longrightarrow \text{M}_{13}$ ) is thermodynamically unfavorable ( $\Delta G = 1.62$  eV). Subsequent reactions to form  $\text{HF}$ ,  $\text{CO}_2$ , and  $\text{PF}_2\text{OOH}$  do not face significant barriers and should occur rapidly. The reaction between  $\text{POF}_3$  and  $\text{LiHCO}_3$  (Figure 3b) follows a similar mechanism. The addition step ( $\text{M}_{16} \longrightarrow \text{M}_{17}$ ) is also endergonic ( $\Delta G^\ddagger = 0.48$  eV,  $\Delta G = 0.52$  eV), though we suggest that it could be ac-

cessed at moderate temperatures. Addition by  $\text{LiHCO}_3$  is followed by the elimination of  $\text{LiF}$  ( $M_{18} \longrightarrow M_{19}$ ), which is analogous to the elimination of  $\text{HF}$  in Figure 3a, ( $M_{13} \longrightarrow M_{14}$ ). Following the complete removal of  $\text{LiF}$ ,  $M_{19}$  can undergo the same concerted proton transfer and  $\text{CO}_2$  elimination shown in Figure 3a ( $M_{14} \longrightarrow M_{15}$ ).

In contrast,  $\text{POF}_3$  adds easily to  $\text{Li}_2\text{CO}_3$  (Figure 3c,  $M_{20} \longrightarrow M_{21}$ ), with  $\Delta G^\ddagger = 0.15$  eV and  $\Delta G = -0.01$  eV. We explain the difference in the thermodynamics of the reactions between  $\text{POF}_3$  and  $\text{H}_2\text{CO}_3$ ,  $\text{LiHCO}_3$ , and  $\text{Li}_2\text{CO}_3$  by considering atomic partial charges (Figure 3d).  $\text{POF}_3$  is reactive towards the highly anionic oxygens in  $\text{Li}_2\text{CO}_3$ , but not towards the less charged oxygens in  $\text{LiHCO}_3$  and  $\text{H}_2\text{CO}_3$ . A similar trend is found for the reaction between  $\text{PF}_5$  and inorganic carbonates (see Supporting Information). Though  $\text{PF}_2\text{OOH}$  formation via  $\text{LiHCO}_3$  is possible, the difficulty of addition with protonated carbonates suggests that, barring electrochemical processes,  $\text{LiPF}_2\text{O}_2$  should be more abundant at the negative electrode than  $\text{PF}_2\text{OOH}$ . Nonetheless, the prediction that  $\text{PF}_2\text{OOH}$  and  $\text{LiPF}_2\text{O}_2$  can form at or near the SEI without the need for cross-talk from the positive electrode motivates further efforts to understand the interactions between these species and other SEI components.

Mechanisms for the reformation of  $\text{POF}_3$  (completing the autocatalytic cycle in Equation 2) are shown in Figure 4. Following a similar trend to that shown in Figure 3d, the attack of  $\text{PF}_5$  by the protonated  $\text{PF}_2\text{OOH}$  (Figure 4a,  $\text{PF}_2\text{OOH} + \text{PF}_5 \longrightarrow M_{25}$ ) is thermodynamically unfavorable, while  $\text{LiPF}_2\text{O}_2$  can favorably add to  $\text{PF}_5$  (Figure 4b,  $\text{LiPF}_2\text{O}_2 + \text{PF}_5 \longrightarrow M_{28}$ ). After the initial addition, an intramolecular fluorine transfer is required; for both  $\text{PF}_2\text{O}_2\text{R}$  species considered, this step is thermodynamically unfavorable and suffers from a high barrier ( $M_{25} \longrightarrow M_{26}$ ,  $\Delta G^\ddagger = 0.95$  eV;  $M_{29} \longrightarrow M_{30}$ ,  $\Delta G^\ddagger = 1.76$  eV). While both intramolecular fluorine transfer reactions are kinetically limited at room temperature (Figure 4 c-d), the reaction without  $\text{Li}^+$  can occur rapidly at elevated temperature (especially  $T > 150^\circ\text{C}$ ). After fluorine transfer, the two mechanisms in Figure 4a-b diverge. In Figure 4a, a concerted proton transfer and elimination step occurs ( $M_{26} \longrightarrow M_{27}$ ), yielding  $\text{POF}_3$  and  $\text{PF}_4\text{OH}$ .  $\text{PF}_4\text{OH}$

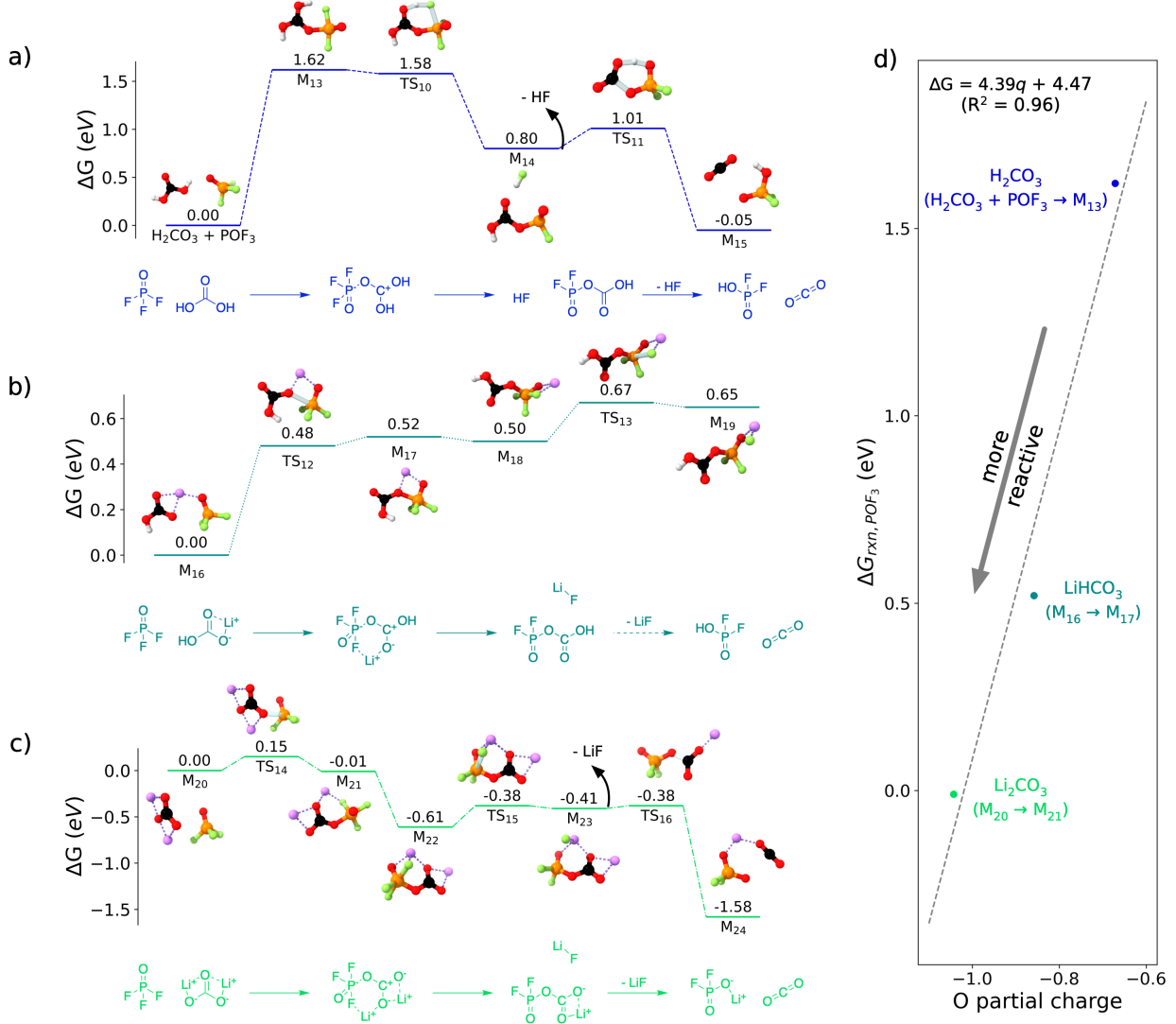


Figure 3: Reactions between  $\text{POF}_3$  and simple inorganic carbonates (a)  $\text{H}_2\text{CO}_3$ , (b)  $\text{LiHCO}_3$ , and (c)  $\text{Li}_2\text{CO}_3$ ) to form  $\text{CO}_2$  and either  $\text{PF}_2\text{OOH}$  or  $\text{LiPF}_2\text{O}_2$ . In (b), the final step to form  $\text{PF}_2\text{OOH}$  from  $M_{19}$  is omitted, as it is identical to the final step in (a) ( $M_{14} \rightarrow M_{15}$ ) with the substitution of LiF as the leaving group rather than HF. A trend between the partial charge of the reacting oxygen(s) (see Supporting Information for details) and the reaction energies with  $\text{POF}_3$  for each carbonate considered is shown in (d). A linear fit,  $\Delta G = 4.39q + 4.47$ , where  $q$  = the most negative oxygen partial charge, shows strong agreement ( $R^2 = 0.96$ ) within the family of inorganic carbonates.

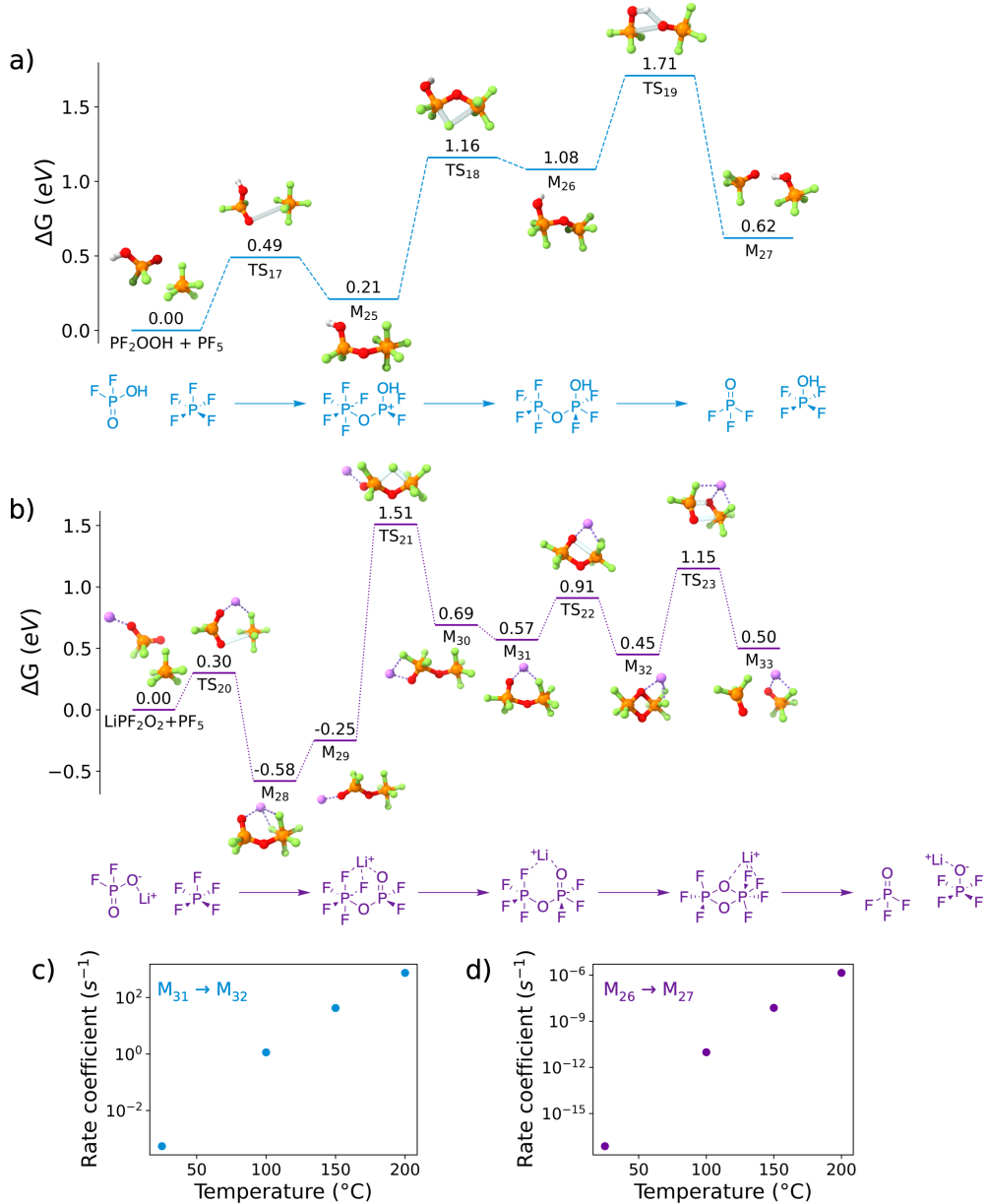


Figure 4: Possible routes for the reformation of  $\text{POF}_3$  from  $\text{PF}_2\text{OOH}$  (a) and  $\text{LiPF}_2\text{O}_2$  (b). Both mechanisms are kinetically limited due to an extremely unfavorable intramolecular fluorine transfer step ( $\text{M}_{25} \rightarrow \text{M}_{26}$ ,  $\text{M}_{29} \rightarrow \text{M}_{30}$ ), which makes  $\text{POF}_3$  autocatalysis unlikely at modest temperatures. Rate coefficients for the fluorine transfer step are provided in c) for the  $\text{PF}_2\text{OOH}$  pathway and in d) for the  $\text{LiPF}_2\text{O}_2$  pathway.

can subsequently eliminate HF to form  $\text{POF}_3$ , as shown in Figure 1. In Figure 4b, a four-member O-P-O-P ring is formed ( $M_{31} \longrightarrow M_{32}$ ) and  $\text{POF}_3$  is eliminated ( $M_{32} \longrightarrow M_{33}$ ), leaving  $\text{LiPOF}_4$  which could then form LiF and  $\text{POF}_3$  as previously discussed.

Our mechanism confirms the previously reported autocatalytic formation of  $\text{POF}_3$ . We find, in agreement with earlier experimental studies,<sup>50,52</sup> that this cycle requires significant thermal activation ( $T \sim 150^\circ\text{C}$ ). This is primarily due to a sluggish intramolecular fluorine transfer and, specifically for the mechanism requiring  $\text{PF}_2\text{OOH}$  as an intermediate, the high barrier for HF elimination to reform  $\text{POF}_3$ . While we have found a mechanism for  $\text{POF}_3$  autocatalysis that does not require any water, the significantly lower barrier for the pathway involving  $\text{PF}_2\text{OOH}$  indicates that  $\text{LiPF}_6$  thermal decomposition could be initiated and accelerated by  $\text{LiPF}_6$  hydrolysis,<sup>47</sup> which is accessible at elevated temperature.

**Conclusions:**  $\text{LiPF}_6$  is an exceptional salt that is likely to play a major role in the LIB market for years to come. While some decomposition of  $\text{LiPF}_6$  is desirable to form a functional SEI, continued breakdown can severely limit the life of LiBs. In this work, we identified a facile elementary decomposition mechanism of  $\text{LiPF}_6$  using first-principles DFT simulations. Our results imply that under normal battery cycling conditions, the major decomposition mechanism of  $\text{LiPF}_6$  does not depend on water or on electrochemical salt reduction. Rather,  $\text{LiPF}_6$  forms the expected products LiF,  $\text{POF}_3$ ,  $\text{LiPF}_2\text{O}_2$ , and potentially  $\text{PF}_2\text{OOH}$  via entirely chemical reactions with inorganic carbonates (especially  $\text{Li}_2\text{CO}_3$ ).  $\text{PF}_5$  and  $\text{POF}_3$  show a strong affinity for highly charged oxyanions, suggesting that efforts to control the reactivity of  $\text{LiPF}_6$  should focus on limiting the exposure of  $\text{PF}_5$  to oxyanion species, including and especially inorganic carbonates like  $\text{Li}_2\text{CO}_3$ , in the SEI as well as on the surface of positive electrodes. This consideration may include morphological control, such as reducing porosity and/or abundance of inorganic species in the outer regions of the SEI. Identification of the primary  $\text{PF}_6^-$  breakdown mechanism will also enable future work including studies of the elementary reaction mechanisms between  $\text{LiPF}_6$  decomposition products (especially  $\text{PF}_2\text{O}_2\text{R}$  species) and other SEI species (e.g. organic carbonates) as well

as the formation mechanisms of organophosphorus compounds and phosphate polymers in the SEI.

## Author Contributions

Conceptualization: E.W.C.S.-S., K.A.P.; Formal analysis: E.W.C.S.-S., T.B.P., H.D.P.; Funding acquisition: E.W.C.S.-S., H.D.P., S.M.B., K.A.P.; Investigation: E.W.C.S.-S., T.B.P., H.D.P.; Resources: K.A.P.; Supervision: E.W.C.S.-S., K.A.P.; Visualization: E.W.C.S.-S.; Writing - original draft: E.W.C.S.-S., T.B.P.; Writing - review & editing: all authors.

## Competing Interests Statement

The authors declare no competing financial interests.

## Acknowledgement

This work is intellectually led by the Silicon Consortium Project directed by Brian Cunningham under the Assistant Secretary for Energy Efficiency and Renewable Energy, Office of Vehicle Technologies of the U.S. Department of Energy, Contract No. DE-AC02-05CH11231 with additional support from the Joint Center for Energy Storage Research, an Energy Innovation Hub funded by the U.S. Department of Energy, Office of Science, Basic Energy Sciences. E.W.C.S.-S. is supported by the Kavli Energy Nanoscience Institute Philomathia Graduate Student Fellowship. H.D.P. is supported by the United States Department of Defense National Defense Science and Engineering Graduate Fellowship. S.M.B. is supported by the Laboratory Directed Research and Development Program of Lawrence Berkeley National Laboratory under U.S. Department of Energy Contract No. DE-AC02-05CH11231. T.B.P. conducted this work as part of the Community College Internship program under the U.S. Department of Energy, Office of Science, Office of Workforce Development for Teach-

ers and Scientists. Access to and assistance using the Schrödinger Suite of software tools, including Jaguar and AutoTS, was generously provided by Schrödinger, Inc. Data for this study was produced using computational resources provided by the Eagle and Swift high-performance computing (HPC) systems at the National Renewable Energy Laboratory and the Lawrencium HPC cluster at Lawrence Berkeley National Laboratory.

## Supporting Information Available

Structural and thermochemical data for all molecules considered in this study; computational methods; discussion of additional reaction mechanisms for LiPF<sub>6</sub> decomposition.

## References

- (1) Li, M.; Lu, J.; Chen, Z.; Amine, K. 30 Years of Lithium-Ion Batteries. *Advanced Materials* **2018**, *30*, 1800561.
- (2) Evers, S.; Nazar, L. F. New Approaches for High Energy Density Lithium–Sulfur Battery Cathodes. *Acc. Chem. Res.* **2013**, *46*, 1135–1143.
- (3) Cheng, X.-B.; Zhang, R.; Zhao, C.-Z.; Zhang, Q. Toward Safe Lithium Metal Anode in Rechargeable Batteries: A Review. *Chem. Rev.* **2017**, *117*, 10403–10473.
- (4) Liu, B.; Zhang, J.-G.; Xu, W. Advancing Lithium Metal Batteries. *Joule* **2018**, *2*, 833–845.
- (5) Voronina, N.; Sun, Y.-K.; Myung, S.-T. Co-Free Layered Cathode Materials for High Energy Density Lithium-Ion Batteries. *ACS Energy Lett.* **2020**, *5*, 1814–1824.
- (6) Kalaga, K.; Rodrigues, M.-T. F.; Trask, S. E.; Shkrob, I. A.; Abraham, D. P. Calendar-life versus cycle-life aging of lithium-ion cells with silicon-graphite composite electrodes. *Electrochimica Acta* **2018**, *280*, 221–228.

- (7) Aurbach, D.; Talyosef, Y.; Markovsky, B.; Markevich, E.; Zinigrad, E.; Asraf, L.; Gnanaraj, J. S.; Kim, H.-J. Design of electrolyte solutions for Li and Li-ion batteries: a review. *Electrochimica Acta* **2004**, *50*, 247–254.
- (8) Logan, E. R.; Dahn, J. R. Electrolyte Design for Fast-Charging Li-Ion Batteries. *Trends in Chemistry* **2020**, *2*, 354–366.
- (9) Li, Q.; Liu, G.; Cheng, H.; Sun, Q.; Zhang, J.; Ming, J. Low-Temperature Electrolyte Design for Lithium-Ion Batteries: Prospect and Challenges. *Chemistry – A European Journal* **2021**, *27*, 15842–15865.
- (10) Blomgren, G. E. Electrolytes for advanced batteries. *Journal of Power Sources* **1999**, *81-82*, 112–118.
- (11) Zhang, S. S.; Jow, T. R.; Amine, K.; Henriksen, G. L. LiPF<sub>6</sub>–EC–EMC electrolyte for Li-ion battery. *Journal of Power Sources* **2002**, *107*, 18–23.
- (12) Xu, K. Nonaqueous Liquid Electrolytes for Lithium-Based Rechargeable Batteries. *Chem. Rev.* **2004**, *104*, 4303–4418.
- (13) Wagner, R.; Preschitschek, N.; Passerini, S.; Leker, J.; Winter, M. Current research trends and prospects among the various materials and designs used in lithium-based batteries. *J Appl Electrochem* **2013**, *43*, 481–496.
- (14) Stich, M.; Göttlinger, M.; Kurniawan, M.; Schmidt, U.; Bund, A. Hydrolysis of LiPF<sub>6</sub> in Carbonate-Based Electrolytes for Lithium-Ion Batteries and in Aqueous Media. *J. Phys. Chem. C* **2018**, *122*, 8836–8842.
- (15) Seo, D. M.; Reininger, S.; Kutcher, M.; Redmond, K.; Euler, W. B.; Lucht, B. L. Role of Mixed Solvation and Ion Pairing in the Solution Structure of Lithium Ion Battery Electrolytes. *J. Phys. Chem. C* **2015**, *119*, 14038–14046.

- (16) Hou, T.; Yang, G.; Rajput, N. N.; Self, J.; Park, S.-W.; Nanda, J.; Persson, K. A. The influence of FEC on the solvation structure and reduction reaction of LiPF<sub>6</sub>/EC electrolytes and its implication for solid electrolyte interphase formation. *Nano Energy* **2019**, *64*, 103881.
- (17) Hou, T.; D. Fong, K.; Wang, J.; A. Persson, K. The solvation structure, transport properties and reduction behavior of carbonate-based electrolytes of lithium-ion batteries. *Chemical Science* **2021**, *12*, 14740–14751.
- (18) Aurbach, D.; Markovsky, B.; Shechter, A.; Ein-Eli, Y.; Cohen, H. A Comparative Study of Synthetic Graphite and Li Electrodes in Electrolyte Solutions Based on Ethylene Carbonate-Dimethyl Carbonate Mixtures. *J. Electrochem. Soc.* **1996**, *143*, 3809.
- (19) Verma, P.; Maire, P.; Novák, P. A review of the features and analyses of the solid electrolyte interphase in Li-ion batteries. *Electrochimica Acta* **2010**, *55*, 6332–6341.
- (20) Agubra, V.; Fergus, J. Lithium Ion Battery Anode Aging Mechanisms. *Materials* **2013**, *6*, 1310–1325.
- (21) Nie, M.; Chalasani, D.; Abraham, D. P.; Chen, Y.; Bose, A.; Lucht, B. L. Lithium Ion Battery Graphite Solid Electrolyte Interphase Revealed by Microscopy and Spectroscopy. *J. Phys. Chem. C* **2013**, *117*, 1257–1267.
- (22) Agubra, V. A.; Fergus, J. W. The formation and stability of the solid electrolyte interface on the graphite anode. *Journal of Power Sources* **2014**, *268*, 153–162.
- (23) Heiskanen, S. K.; Kim, J.; Lucht, B. L. Generation and Evolution of the Solid Electrolyte Interphase of Lithium-Ion Batteries. *Joule* **2019**, *3*, 2322–2333.
- (24) Cheng, X.-B.; Zhang, R.; Zhao, C.-Z.; Wei, F.; Zhang, J.-G.; Zhang, Q. A Review of Solid Electrolyte Interphases on Lithium Metal Anode. *Advanced Science* **2016**, *3*, 1500213.

- (25) Xue, W.; Shi, Z.; Huang, M.; Feng, S.; Wang, C.; Wang, F.; Lopez, J.; Qiao, B.; Xu, G.; Zhang, W.; Dong, Y.; Gao, R.; Shao-Horn, Y.; A. Johnson, J.; Li, J. FSI-inspired solvent and “full fluorosulfonyl” electrolyte for 4 V class lithium-metal batteries. *Energy & Environmental Science* **2020**, *13*, 212–220.
- (26) Nie, M.; Abraham, D. P.; Chen, Y.; Bose, A.; Lucht, B. L. Silicon Solid Electrolyte Interphase (SEI) of Lithium Ion Battery Characterized by Microscopy and Spectroscopy. *J. Phys. Chem. C* **2013**, *117*, 13403–13412.
- (27) Philippe, B.; Dedryvère, R.; Gorgoi, M.; Rensmo, H.; Gonbeau, D.; Edström, K. Improved Performances of Nanosilicon Electrodes Using the Salt LiFSI: A Photoelectron Spectroscopy Study. *J. Am. Chem. Soc.* **2013**, *135*, 9829–9842.
- (28) McBrayer, J. D. et al. Calendar aging of silicon-containing batteries. *Nat Energy* **2021**, *6*, 866–872.
- (29) Boyle, D. T.; Huang, W.; Wang, H.; Li, Y.; Chen, H.; Yu, Z.; Zhang, W.; Bao, Z.; Cui, Y. Corrosion of lithium metal anodes during calendar ageing and its microscopic origins. *Nat Energy* **2021**, *6*, 487–494.
- (30) Aurbach, D.; Ein-Eli, Y.; Markovsky, B.; Zaban, A.; Luski, S.; Carmeli, Y.; Yamin, H. The Study of Electrolyte Solutions Based on Ethylene and Diethyl Carbonates for Rechargeable Li Batteries: II . Graphite Electrodes. *J. Electrochem. Soc.* **1995**, *142*, 2882.
- (31) Aurbach, D.; Zaban, A.; Schechter, A.; Ein-Eli, Y.; Zinigrad, E.; Markovsky, B. The Study of Electrolyte Solutions Based on Ethylene and Diethyl Carbonates for Rechargeable Li Batteries: I . Li Metal Anodes. *J. Electrochem. Soc.* **1995**, *142*, 2873.
- (32) Winter, M. The Solid Electrolyte Interphase – The Most Important and the Least Understood Solid Electrolyte in Rechargeable Li Batteries. *Zeitschrift für Physikalische Chemie* **2009**, *223*, 1395–1406.

- (33) Rowden, B.; Garcia-Araez, N. A review of gas evolution in lithium ion batteries. *Energy Reports* **2020**, *6*, 10–18.
- (34) Zhao, H.; Wang, J.; Shao, H.; Xu, K.; Deng, Y. Gas Generation Mechanism in Li-Metal Batteries. *Energy & Environmental Materials* **2022**, *5*, 327–336.
- (35) Ma, Y.; Balbuena, P. B. DFT Study of Reduction Mechanisms of Ethylene Carbonate and Fluoroethylene Carbonate on Li+-Adsorbed Si Clusters. *J. Electrochem. Soc.* **2014**, *161*, E3097.
- (36) Gibson, L. D.; Pfaendtner, J. Solvent oligomerization pathways facilitated by electrolyte additives during solid-electrolyte interphase formation. *Phys. Chem. Chem. Phys.* **2020**, *22*, 21494–21503.
- (37) Kuai, D.; Balbuena, P. B. Solvent Degradation and Polymerization in the Li-Metal Battery: Organic-Phase Formation in Solid-Electrolyte Interphases. *ACS Appl. Mater. Interfaces* **2022**, *14*, 2817–2824.
- (38) Leung, K.; Budzien, J. L. Ab initio molecular dynamics simulations of the initial stages of solid–electrolyte interphase formation on lithium ion battery graphitic anodes. *Phys. Chem. Chem. Phys.* **2010**, *12*, 6583–6586.
- (39) Soto, F. A.; Ma, Y.; Martinez de la Hoz, J. M.; Seminario, J. M.; Balbuena, P. B. Formation and Growth Mechanisms of Solid-Electrolyte Interphase Layers in Rechargeable Batteries. *Chem. Mater.* **2015**, *27*, 7990–8000.
- (40) Young, J.; Kulick, P. M.; Juran, T. R.; Smeu, M. Comparative Study of Ethylene Carbonate-Based Electrolyte Decomposition at Li, Ca, and Al Anode Interfaces. *ACS Appl. Energy Mater.* **2019**, *2*, 1676–1684.
- (41) M. Blau, S.; D. Patel, H.; Clark Spotte-Smith, E. W.; Xie, X.; Dwaraknath, S.; A. Pers-

- son, K. A chemically consistent graph architecture for massive reaction networks applied to solid-electrolyte interphase formation. *Chemical Science* **2021**, *12*, 4931–4939.
- (42) Xie, X.; Clark Spotte-Smith, E. W.; Wen, M.; Patel, H. D.; Blau, S. M.; Persson, K. A. Data-Driven Prediction of Formation Mechanisms of Lithium Ethylene Monocarbonate with an Automated Reaction Network. *J. Am. Chem. Soc.* **2021**, *143*, 13245–13258.
- (43) Barter, D.; Spotte-Smith, E. W. C.; Redkar, N. S.; Khanwale, A.; Dwaraknath, S.; Persson, K. A.; Blau, S. M. Predictive stochastic analysis of massive filter-based electrochemical reaction networks. *ChemRxiv* **2022**, DOI: 10.26434/chemrxiv-2021-c2gp3-v3.
- (44) Spotte-Smith, E. W. C.; Kam, R. L.; Barter, D.; Xie, X.; Hou, T.; Dwaraknath, S.; Blau, S. M.; Persson, K. A. Toward a Mechanistic Model of Solid-Electrolyte Interphase Formation and Evolution in Lithium-Ion Batteries. *ACS Energy Lett.* **2022**, *7*, 1446–1453.
- (45) Sloop, S. E.; Pugh, J. K.; Wang, S.; Kerr, J. B.; Kinoshita, K. Chemical Reactivity of PF 5 and LiPF6 in Ethylene Carbonate/Dimethyl Carbonate Solutions. *Electrochem. Solid-State Lett.* **2001**, *4*, A42.
- (46) Kawamura, T.; Okada, S.; Yamaki, J.-i. Decomposition reaction of LiPF6-based electrolytes for lithium ion cells. *Journal of Power Sources* **2006**, *156*, 547–554.
- (47) Yang, H.; Zhuang, G. V.; Ross, P. N. Thermal stability of LiPF6 salt and Li-ion battery electrolytes containing LiPF6. *Journal of Power Sources* **2006**, *161*, 573–579.
- (48) Wiemers-Meyer, S.; Winter, M.; Nowak, S. Mechanistic insights into lithium ion battery electrolyte degradation – a quantitative NMR study. *Physical Chemistry Chemical Physics* **2016**, *18*, 26595–26601.
- (49) Henschel, J.; Peschel, C.; Klein, S.; Horsthemke, F.; Winter, M.; Nowak, S. Clarification of Decomposition Pathways in a State-of-the-Art Lithium Ion Battery Elec-

- trolyte through  $^{13}\text{C}$ -Labeling of Electrolyte Components. *Angewandte Chemie* **2020**, *132*, 6184–6193.
- (50) Botte, G. G.; White, R. E.; Zhang, Z. Thermal stability of LiPF<sub>6</sub>–EC:EMC electrolyte for lithium ion batteries. *Journal of Power Sources* **2001**, *97*–*98*, 570–575.
- (51) Lux, S. F.; Lucas, I. T.; Pollak, E.; Passerini, S.; Winter, M.; Kostecki, R. The mechanism of HF formation in LiPF<sub>6</sub> based organic carbonate electrolytes. *Electrochemistry Communications* **2012**, *14*, 47–50.
- (52) Campion, C. L.; Li, W.; Lucht, B. L. Thermal Decomposition of LiPF<sub>6</sub>-Based Electrolytes for Lithium-Ion Batteries. *J. Electrochem. Soc.* **2005**, *152*, A2327.
- (53) Wagner, R.; Korth, M.; Streipert, B.; Kasnatscheew, J.; Gallus, D. R.; Brox, S.; Amereller, M.; Cekic-Laskovic, I.; Winter, M. Impact of Selected LiPF<sub>6</sub> Hydrolysis Products on the High Voltage Stability of Lithium-Ion Battery Cells. *ACS Appl. Mater. Interfaces* **2016**, *8*, 30871–30878.
- (54) Okamoto, Y. Ab Initio Calculations of Thermal Decomposition Mechanism of LiPF<sub>6</sub>-Based Electrolytes for Lithium-Ion Batteries. *J. Electrochem. Soc.* **2013**, *160*, A404.
- (55) Gebala, A. E.; Jones, M. M. The acid catalyzed hydrolysis of hexafluorophosphate. *Journal of Inorganic and Nuclear Chemistry* **1969**, *31*, 771–776.
- (56) Rinkel, B. L. D.; Hall, D. S.; Temprano, I.; Grey, C. P. Electrolyte Oxidation Pathways in Lithium-Ion Batteries. *J. Am. Chem. Soc.* **2020**, *142*, 15058–15074.
- (57) Liu, M.; Vatamanu, J.; Chen, X.; Xing, L.; Xu, K.; Li, W. Hydrolysis of LiPF<sub>6</sub> - Containing Electrolyte at High Voltage. *ACS Energy Lett.* **2021**, *6*, 2096–2102.
- (58) Cao, C.; Pollard, T. P.; Borodin, O.; Mars, J. E.; Tsao, Y.; Lukatskaya, M. R.; Kasse, R. M.; Schroeder, M. A.; Xu, K.; Toney, M. F.; Steinrück, H.-G. Toward Unrav-

eling the Origin of Lithium Fluoride in the Solid Electrolyte Interphase. *Chem. Mater.* **2021**, *33*, 7315–7336.

- (59) Bi, Y.; Wang, T.; Liu, M.; Du, R.; Yang, W.; Liu, Z.; Peng, Z.; Liu, Y.; Wang, D.; Sun, X. Stability of Li<sub>2</sub>CO<sub>3</sub> in cathode of lithium ion battery and its influence on electrochemical performance. *RSC Adv.* **2016**, *6*, 19233–19237.
- (60) Parimalam, B. S.; MacIntosh, A. D.; Kadam, R.; Lucht, B. L. Decomposition Reactions of Anode Solid Electrolyte Interphase (SEI) Components with LiPF<sub>6</sub>. *J. Phys. Chem. C* **2017**, *121*, 22733–22738.
- (61) Leung, K. Two-electron reduction of ethylene carbonate: A quantum chemistry re-examination of mechanisms. *Chemical Physics Letters* **2013**, *568-569*, 1–8.
- (62) An, S. J.; Li, J.; Daniel, C.; Mohanty, D.; Nagpure, S.; Wood, D. L. The state of understanding of the lithium-ion-battery graphite solid electrolyte interphase (SEI) and its relationship to formation cycling. *Carbon* **2016**, *105*, 52–76.
- (63) Jayawardana, C.; Rodrigo, N.; Parimalam, B.; Lucht, B. L. Role of Electrolyte Oxidation and Difluorophosphoric Acid Generation in Crossover and Capacity Fade in Lithium Ion Batteries. *ACS Energy Lett.* **2021**, *6*, 3788–3792.
- (64) Jayawardana, C.; Rodrigo, N. D.; Rynearson, L.; Lucht, B. L. Difluorophosphoric Acid Generation and Crossover Reactions in LiNi<sub>x</sub>CoyMnzO<sub>2</sub> Cathodes Operating at High Voltage. *J. Electrochem. Soc.* **2022**, *169*, 060509.

## For Table of Contents Only

